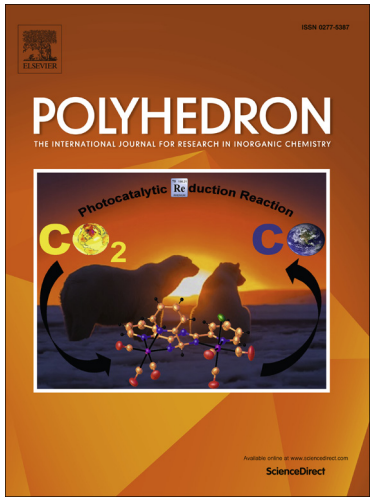

Novel chelate complexes of Co(II), Ni(II), Cu(II), Pd(II) derived from *anti*- and *syn*-isomers of 2-(2-aminothiazole-4-yl)-2-hydroxyiminoacetic acid with pro-/antiproliferative actions on endothelial cells

S.I. Orysyk, O.O. Zholob, V.V. Bon, V.V. Nikulina, V.V. Orysyk, T.V. Nikolaienko, L.V. Garmanchuk, Yu.L. Zborovskii, G.M. Tolstanova, N.N. Khranovskaya, V.I. Pekhnyo, M.V. Vovk

PII: S0277-5387(14)00556-7
DOI: http://dx.doi.org/10.1016/j.poly.2014.08.034
Reference: POLY 10935

To appear in: *Polyhedron*

Received Date: 12 May 2014
Accepted Date: 2 August 2014

Please cite this article as: S.I. Orysyk, O.O. Zholob, V.V. Bon, V.V. Nikulina, V.V. Orysyk, T.V. Nikolaienko, L.V. Garmanchuk, Yu.L. Zborovskii, G.M. Tolstanova, N.N. Khranovskaya, V.I. Pekhnyo, M.V. Vovk, Novel chelate complexes of Co(II), Ni(II), Cu(II), Pd(II) derived from *anti*- and *syn*-isomers of 2-(2-aminothiazole-4-yl)-2-hydroxyiminoacetic acid with pro-/antiproliferative actions on endothelial cells, *Polyhedron* (2014), doi: http://dx.doi.org/10.1016/j.poly.2014.08.034

Novel chelate complexes of Co(II), Ni(II), Cu(II), Pd(II) derived from *anti*- and *syn*-isomers of 2-(2-aminothiazole-4-yl)-2-hydroxyiminoacetic acid with pro-/antiproliferative actions on endothelial cells

S.I. Orysyk[a1], O.O. Zholob[a], V.V. Bon[b], V.V. Nikulina[c], V.V. Orysyk[d], T.V. Nikolaienko[c], L.V. Garmanchuk[c], Yu.L. Zborovskii[d], G.M. Tolstanova[c], N.N. Khranovskaya[e], V.I. Pekhnyo[a], M.V. Vovk[d].

[a] *V.I. Vernadskii Institute of General and Inorganic Chemistry NAS of Ukraine, Palladin Ave. 32/34, 03680 Kyiv, Ukraine*

[b] *Department of Inorganic Chemistry, Dresden University of Technology, Bergstrasse 66, 01069 Dresden, Germany*

[c] *Educational and Scientific Centre "Institute of Biology" of Taras Shevchencko National University, Glushkov Ave. 2, 03022 Kyiv, Ukraine*

[d] *Institute of Organic Chemistry NAS of Ukraine, Murmanska str. 5, 02660 Kyiv, Ukraine*

[e] *National Cancer Institute, Lomonosov str., 33/43, 03022 Kyiv, Ukraine*

Abstract

Anti- and *syn*-isomers of 2-(2-aminothiazole-4-yl)-2-hydroxyiminoacetic acid (*anti*-A and *syn*-A respectively) were used as potential biologically active polydentate complexing agent for Co^{2+}, Ni^{2+}, Cu^{2+} and Pd^{2+} ions for the synthesis of novel complex compounds with directed angiogenesis-correcting action. It shown that the location of functional groups in ligand molecules, the electronic structure of metal as complexing agent and the synthesis conditions affect the localization of coordination bonds and the structure of formed complexes. The interaction of ethanol solutions of metal salts with *anti*-A and *syn*-A in an acidic medium at the component ratios M:L=1:1 and 1:2 leads to the formation of complexes [Co(*anti*-A)$(H_2O)_3SO_4$] (**1**); [Ni(*anti*-A)$(H_2O)_3SO_4$] (**2**); [Cu(*anti*-A)$_2Cl_2$] (**3**); [Pd(*anti*-A)$_2Cl_2$] (**4**); [Cu(*syn*-A)$_2Cl_2$] (**5**); [Pd(*syn*-A)Cl_2] (**6**) with different coordination of ligands. Coordination mode of ligands identified by IR, UV-Vis, XPS and ^1H (^{13}C) NMR spectra. The structures of salt of the *anti*-A and complexes 1, 2, 6 were determined by X-ray diffraction study. *Anti*-A is coordinated to metal ions in a chelate manner by the nitrogen atom of the hydroxylimino group and the oxygen atom of the deprotonated carboxyl group. In this case, the 2-aminothiazole fragment does not involve in complexation. *Syn*-A is

[1] Author for correspondence. Tel.: +38(044)4240511; +38(095)3533288; fax: +380(44)4243070

E-mail address: s_oryslend@mail.ru (S.I. Orysyk)

coordinated to the central metal ion in neutral form through the nitrogen atoms of hydroxyimino group and thiazole ring. All synthesized complex compounds form stable solutions in neutral medium, which makes it possible to use them as potential biologically active substances.

Investigation of biological effects for *syn*-A shows mitogenic and antiapoptotic activity against endotheliocytes, while *anti*-A causes inhibition of proliferation almost in the entire concentration range. Complex compounds of Cu^{2+} and Pd^{2+} with *anti*-A and *syn*-A (**3–6)** cause an increase of antiproliferative activity of endothelial cells compared with baseline complexing agents. In this case, the activity of complexes with *syn*-A is superior to activity of analogues with *anti*-A. The results of cytotoxicity tests revealed a pronounced cytotoxic action for complexes **3** and **4,** cytotoxic and proapoptotic activity for **6** and cytostatic effect for **5.** For all compounds investigated, a checkpoint from S to G_2 has been established, which may indicate DNA replication disturbance or dysregulation in the endogeneous signals of the cell cycle of endotheliocytes.

Keywords: hydroxyiminoacetates, transition metal complexes, X-Ray diffraction study, pro- and antiproliferative actions, endothelial cell proliferation

1. Introduction

The development of complex compounds based on biologically active organic ligands has become a promising trend in pharmaceutical chemistry in the recent 10-15 years. Complex formation prevents hydrolysis of inorganic salts in physiologic media, reduces toxicity and facilitates the penetration of drugs through cell membranes. Moreover, the pharmacological characteristics of the complexes are more effective as compared to their initial components [1-4].

Herein we used *Anti-* and *syn*-isomers of 2-(2aminothiazole-4-yl)-2-hydroxyiminoacetic acid (*anti*-A and *syn*-A) as potential biologically active polydentate complexing agents in the synthesis of novel coordination compounds with Cu(II), Co(II), Ni(II) and Pd(II). These ligands contain biologically active fragments of 2-iminothiazole and hydroxyiminoacetic acid that are involved in many biologically active compounds with antibacterial [5, 6] and antiprion [8] properties, and are used as scaffold in medical chemistry to obtain potential pharmaceuticals [5-9]. They are inhibitors of interleukin-2-inducible T cell kinases) [9].

Angiogenesis is known as a multi-step process which consists of remodeling of extracellular matrix, proliferation and migration of endothelial cells, tube formation and blood vessels stabilization [10]. It is regulated by a well-

orchestrated balance between pro- and anti-angiogenic factors. Dysregulated angiogenesis is hallmarks of cancer, ischemic diseases and many chronic inflammatory diseases (e.g., gastrointestinal ulceration, cancer, diabetic retinopathy, atherosclerosis, rheumatoid arthritis) [10-16]. Preclinical and initial clinical evidence reveals that normalization of the vascular abnormalities is emerging as a complementary therapeutic paradigm for cancer and other vascular disorders, which affect more than half a billion people worldwide [10]. Available therapeutic approaches to block or increase vascular supply have reached the clinic, but limited efficacy and resistance pose new challenges

Hypoxia-inducible factor 1 (HIF-1) is a master regulator of hypoxic/ischemic vascular responses, driving transcriptional activation of many genes encoding angiogenic cytokines and growth factors involved in vascular reactivity, angiogenesis, and the mobilization and homing of bone marrow-derived angiogenic cells. HIF-1 plays the pivotal role in vascular homeostasis and involves in vascular diseases [17]. HIF-1 activity manipulation is the perspective therapeutic approach which might overcome the current limitations of pro- and antiangiogenic medicine. Recently the 2-hydroxyimino-2-phenylacetic acid derivatives are reported as efficient HIF-1 inhibitors [18].

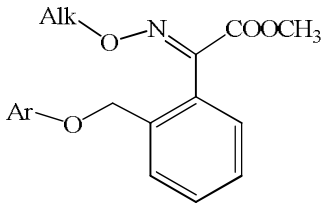

The high bioactivity of these compounds and other 2-hydroxyiminoacetic acid derivatives is explained by their ability to form chelate complexes with many transition metals ions [19, 20]. Polyfunctional 2-hydroxyiminoacetic acids, coordinated to functional groups of peptide fragments in biological media, are able to bind metal ions into stable complexes, and act therefore as inhibitors of metal-containing enzymes and proteins. For instance, a number of amides of 2-hydroxyiminoalkanecarboxylic acid are inhibitors of zinc-containing enzymes (histone deacetylases), that increase their high anticancer activity [21].

The effect of copper and palladium complexes on the proliferation of endothelial cells has been studied. Moreover, the influence of *anti/syn* isomerism both on the complexation reactions and biological activity of coordination compounds has been established.

2. Materials and methods

2.1. Materials and chemicals

All solvents and reagents were purchased from commercial sources and directly used without additional purification. Initial reagents $Co(NO_3)_2 \cdot 6H_2O$ (20.25% Co), $Ni(NO_3)_2 \cdot 6H_2O$ (20.18% Ni), $CuCl_2 \cdot 2H_2O$ (37.28% Cu), $PdCl_2$ (59% Pd), used for the synthesis of complexes, were purchased from Merck.

2.2. Preparation of ligands and metal complexes

2.2.1. 2-(2-Aminothiazole-4-yl)-2-(anti)-hydroxyiminoacetic acid (*anti-A*) and *2-(2-aminothiazole-4-yl)-2-(syn)-hydroxyiminoacetic acid* (*syn-A*)

To a solution of NaOH (2.4 g, 0.06 mol) in water (100 mL) was added ethyl 2-(2-aminothiazole-4-yl)-2-(*anti*)-hydroxyiminoacetate [22] or ethyl 2-(2-aminothiazole-4-yl)-2-(*syn*)-hydroxyiminoacetate [23] (10.76 g, 0.05 mol) with stirring in an ice bath. The mixture was stirred for 2-3 h at 15-20 ^{o}C, after that the solvent was removed in vacuum. The solid residue was dissolved in H_2O (100 mL), treated with Norit (1.0 g) and filtered. The glacial acetic acid was added dropwise to the filtrate with stirring till neutral reaction. The resulting precipitate was filtered off, washed with water and recrystallized twice from the ethanol.

(*Anti-A*). Yield: 6.45 g (69 %), m.p. 186–187 ^{o}C. Anal. Calc. for $C_5H_5N_3O_3S$: C, 32.08; H, 2.69; N, 22.45; S, 17.13; Found: C, 31.94; H, 2.82; N, 22.39; S, 17.09%. ^{1}H NMR (300 MHz; *d*$_6$-DMSO; δ/ppm): 7.30 (br. s, 2H, NH_2); 7.56 (s, 1H, $CH_{thiazole}$); ~12.91 (br. s, OH + COOH). ^{13}C NMR (125.71 MHz; *d*$_6$-DMSO; δ/ppm): 114.48 C(5); 138.04 C(3); 144.01 C(1); 164.85 C(2); 166.82 C(4). IR data, ν, cm^{-1}: 3620 (br. m) ν(OH); 3250 (br. m) $\nu(NH)_{NH2}$; 3180 (m) $\nu(OH)_{C=N-OH}$; 2935 (m) $\nu(C-H)_{thiazole}$; 2780 (w) $(OH)_{COOH}$; 1654 (s) ν(C=O); 1635 (m) $\nu(C=N)_{imine}$; 1575 (br. m) δ(NH); 1530 (m) $\nu(C=N)_{thiazole}$; 1435 (m) $\nu(CH-S)_{thiazole}$; 1367 (m) $\nu(C=C)_{thiazole}$; 1220 (w) ν(C–OH); 1021 (m) ν(N–O); 970 (w), 913 (m) δ(C–H); 823 (m) ν(C–C); 773 (m) δ(C–H); 641 (w), 620 (w), 556 (m), 484 (w), 423 (m) δ(C–C). To obtain the crystals of *anti*-A suitable for single crystal X-ray diffraction study, the compound was crystallized in 0.4M solution of H_2SO_4, resulting in the sulfate salt of *anti*-A. The crystal structure of latter is discussed in the section of X-ray Diffraction Studies.

(*Syn-A*). Yield: 6.67 g (71 %), m.p. 206–207 ^{o}C. Anal. Calc. for $C_5H_5N_3O_3S$: C, 32.08; H, 2.69; N, 22.45; S, 17.13; Found: C, 31.97; H, 2.76; N, 22.31; S, 17.21%. ^{1}H NMR (300 MHz; *d*$_6$-DMSO; δ/ppm): 6.84 (s, 1H, $CH_{thiazole}$) 7.30 (br. s, 2H, NH_2); ~12.43 (br. s, OH + COOH). ^{13}C NMR (125.71 MHz; *d*$_6$-DMSO; δ/ppm): 106.03 C(5); 141.89 C(3); 147.58 C(1); 164.72 C(2); 168.61 C(4). IR data,

ν, cm–1: 3620 (br. m) ν(OH); 3300 (br. m) $\nu(NH)_{NH2}$; 3150 (br. m) $\nu(OH)_{C=N-OH}$; 3025 (br. m) $\nu(C\text{-}H)_{thiazole}$; 2785 (w) $(OH)_{COOH}$; 1665 (s) ν(C=O); 1615 (m) $\nu(C=N)_{imine}$; 1525 (s) $\nu(C=N)_{thiazole}$; $\delta(NH)_{NH2}$; 1430 (s) $\nu(CH-S)_{thiazole}$; 1350 (br. m) $\nu(C=C)_{thiazole}$; 1275 (m) ν(C−N); 1164 (m), 1065 (s) ν(C−OH); 1025 (m) ν(N−O); 888 (m) δ(C−H); 830 (s) ν(C−C); 785 (m), 757 (m) δ(C−H); 688 (m) δ(N−O); 641 (w), 620 (w), 567 (m), 477 (w), 428 (br. s) δ(C−C)

2.2.2. Complex [Co(anti-A)(H₂O)₃SO₄] (**1**)

The compound *anti*-A (0.178 g, 1 mmol) was dissolved in 2M H_2SO_4 (9 mL), and ethanol (5 mL) was added. To the resulting transparent solution heated to 60 – 70 °C a solution of $Co(NO_3)_2 \cdot 6H_2O$ (0.291 g, 1 mmol) in ethanol (10 mL) was added with stirring. The reaction mixture was stirred for 75 min under reflux and cooled down to the room temperature. The pink crystals were formed after 2 days of staying. The pink crystals are filtered off and dried in a vacuum desiccator over $CaCl_2$. Yield: 0.29 g (72 %), m.p. ≥ 250 °C (decomp.). Anal. Calc. for $C_5H_{11}CoN_3O_{10}S_2$: C, 15.16; H, 2.80; N, 10.61; S, 16.19; Found: C, 15.32; H, 3.02; N, 10.52; S, 16.15%. IR data, ν, cm^{-1}: 3620 (br. m) intramolecular hydrogen bond; 3420 (m) $\nu(OH)_{H2O}$; 3200 (m) $\nu(NH)_{NH2}$; 3130 (m) $\nu(OH)_{C=N-OH}$; 3005 (br. m) $\nu(C\text{-}H)_{thiazole}$; 2755 (m) ν(OH) related to intramolecular hydrogen bond; 2617 (br. m) $\nu(NH^+)_{thiazole}$; 1640 (s) ν(C=O); 1610 (m) $\nu(C=N)_{imine}$; 1574 (m) $\nu(C=N)_{thiazole,\ \delta NH}$; 1472 (w) $\nu(CH-S)_{thiazole}$; 1395 (m) $\nu(C=C)_{thiazole}$; 1217 (m) ν(C−OH); 1145 (m); 1085 (br. s) $\nu_3(F_2)\ SO_4^{2-}$; 1060 (m), 983 (w), 963 (w), 870 (m), 785 (m) δ(C−H); 700 (w), 632 (w), 590 (m) $\nu_4(F_2)\ SO_4^{2-}$; 535 (br. w) ν(Co−O); 470 (w), 450 (m) ν(Co−N)

2.2.3. Complex [Ni(anti-A)(H₂O)₃SO₄] (**2**)

$Ni(NO_3)_2 \cdot 6H_2O$ (0.2907 g, 1 mmol) was dissolved in ethanol (10 mL) at 40–50 °C. To the resulted solution, the solution of *anti*-A (0.1872 g, 1 mmol), dissolved in 2M H_2SO_4 (9 mL) was added with stirring. The reaction mixture was stirred for 45 minutes under reflux and cooled down to the room temperature. The cyan crystals were formed after 2 days of staying. The turquoise crystals are then filtered off and dried in a vacuum desiccator over $CaCl_2$.Yield: 0.26 g (65 %), m.p. ≥ 205 °C (decomp.). Anal. Calc. for $C_5H_{11}N_3NiO_{10}S_2$: C, 15.17; H, 2.80; N, 10.61; S, 16.20; Found: C, 15.25; H, 3.08; N, 10.67; S, 16.18%. IR data, ν, cm^{-1}: 3620 (br. m) intramolecular hydrogen bond; 3400 (br. m) $\nu(OH)_{H2O}$; 3312 (m) $\nu(NH)_{NH2}$; 3185 (m) $\nu(OH)_{C=N-OH}$; 3000 (br. m) $\nu(C\text{-}H)_{thiazole}$; 2750 (m) ν(OH) related to intramolecular hydrogen bond; 2650 (br. m) $\nu(NH^+)_{thiazole}$; 1630 (s) ν(C=O); 1620 (m) $\nu(C=N)_{imine}$; 1560 (m) $\nu(C=N)_{thiazole}$ δ(NH); 1485 (m) $\nu(CH-S)_{thiazole}$; 1373 (s) $n\nu(C=C)_{thiazole}$; 1208 (m) ν(C−OH); 1140 (br. s), 1100 (br. s) $\nu_3(F_2)\ SO_4^{2-}$; 1065 (s),

960 (m), 932 (m), 800 (m) δ(C–H); 730 (br. m), 618 (m) $\nu_4(F_2)$ SO_4^{2-}; 555 (m), 505 (m) ν(Ni–O); 438 (m) ν(Ni–N).

2.2.4. Complex [Cu(anti-A)$_2$Cl$_2$] (**3**)

$CuCl_2 \cdot 2H_2O$ (0.0852 g, 0.5 mmol) was dissolved in ethanol (20 mL) at 40–45 °C. To the resulted solution a solution of *anti*-A (0.0936 g, 0.5 mmol), dissolved in ethanol (10 mL) and 2N HCl (5 mL), heated to 40–45 °C was added dropwise with stirring at the same temperature for 45 minutes. After the cooling of resulted dark olive solution to the room temperature, a dark brown amorphous precipitate was formed. The precipitate was filtered off after 24 hours, washed with ethanol and dried in a vacuum desiccator over $CaCl_2$. Yield: 0.0572 g (45 %), m.p. ≥ 240 °C (decomp.). Anal. Calc. for $C_{10}H_{10}Cl_2CuN_6O_6S_2$: C, 23.61; H, 1.98; Cl, 13.94; N, 16.52; S, 12.60; Found: C, 23.52; H, 2.05; Cl, 14.06; N, 16.48; S, 12.69%. IR data, ν, cm^{-1}: 3620 (br. m) intramolecular hydrogen bond; 3346 (br. m) $\nu(NH)_{NH2}$; 3153 (m) $\nu(OH)_{C=N-OH}$; 3020 (m) $\nu(C\text{-}H)_{thiazole}$; 2680 (m) $\nu(NH^+)_{thiazole}$; 1651 (s) ν(C=O); 1610 (m) $\nu(C{=}N)_{imine}$; 1545 (m) $\nu(C{=}N)_{thiazole}$; 1400 (m) $\nu(CH{-}S)_{thiazole}$; 1358 (m) $\nu(C{=}C)_{thiazole}$; 1292 (w), 1208 (m) ν(–C–N–); 1071 (m) ν(N–O); 980 (m), 815 (m) ν(C–C); 787 (s) δ(C–H); 515 (br. m) ν(Cu–O); 410 (m) ν(Cu–N).

2.2.5. Complex [Pd(anti-A)$_2$Cl$_2$] (**4**)

$PdCl_2$ (0.0266 g, 0.15 mmol) was dissolved in 2N HCl (4 mL) at 40–50 °C, and ethanol (10 mL) was added. To the resulting light brown solution a hot solution of *anti*-A (0.0562 g, 0.3 mmol), dissolved in ethanol (10 mL), and 2N HCl (2 mL) was added dropwise. The reaction mixture was heated for another 50 minutes. The light yellow precipitate that formed after cooling was filtered off, washed with ethanol and diethyl ether and dried in a vacuum desiccator over $CaCl_2$. Yield: 0.0494 g (88 %), m.p. ≥ 283 °C (decomp.). Anal. Calc. for $C_{10}H_{10}Cl_2N_6O_6PdS_2$: C, 21.77; H, 1.83; Cl, 12.85; N, 15.23; S, 11.62; Found: C, 21.95; H, 1.88; Cl, 12.05; N, 15.11; S, 11.23%. ^{1}H NMR, (500 MHz; *d$_6$*-DMSO; δ/ppm): 7.42 (br. s 2H, NH_2); 7.67 (s 1H, $CH_{thiazolyl}$); 8.17 (br. s 1H, NH^+); 9.25 (br. s 1H, OH). ^{13}C NMR (125.71 MHz; *d$_6$*-DMSO; δ/ppm): 116.05 C(5); 140.32 C(3); 142.41 C(1); 160.17 C(2); 172.62 C(4). IR data, ν, cm^{-1}: 3342 (br. m) $\nu(NH)_{NH2}$; 3154 (m) $\nu(OH)_{C=N-OH}$; 2994 (br. m) $\nu(C\text{-}H)_{thiazole}$; 2690 (m) $\nu(NH^+)_{thiazole}$; 1645 (s) ν(C=O); 1615 (m) $\nu(C{=}N)_{imine}$; 1580 (m) $\nu(C{=}N)_{thiazole}$; 1404 (m) $\nu(CH{-}S)_{thiazole}$; 1355 (m) $\nu(C{=}C)_{thiazole}$; 1193 (m) ν(–C–N–); 1075 (m) ν(N–O); 823 (m)ν(C–C), 788 (s) δ(C–H), 530 (br. m) ν(Pd–O), 404 (m) ν(Pd–N).

2.2.6. Complex [Cu(syn-A)$_2$Cl$_2$] (**5**)

$CuCl_2 \cdot H_2O$ (0.0852 g, 0.5 mmol) was dissolved with stirring in ethanol (25 mL) at 40–50 °C. To the resulted solution a solution of *syn*-A (0.1872 g, 1 mmol), dissolved in 4N HCl (10 mL), and ethanol (20 mL) was added. The reaction mixture was stirred for 2 h under reflux and cooled down to the room temperature, resulting in the formation of the dark green amorphous precipitate, which was filtered off, washed with ethanol and diethyl ether and dried in a vacuum desiccator over $CaCl_2$. Yield: 0.229 g (90 %), m.p. ≥ 215 °C (decomp.). Anal. Calc. for $C_{10}H_{10}Cl_2CuN_6O_6S_2$: C, 23.61; H, 1.98; Cl, 13.94; N, 16.52; S, 12.60; Found: C, 23.55; H, 2.15; Cl, 13.75; N, 16.45; S, 12.53 %. IR data, ν, cm^{-1}: 3600 (br. m) intramolecular hydrogen bond; 3321 (m) $\nu(OH)_{COOH}$; 3235 (m) $\nu(NH)_{NH2}$; 3070 (br. m) $\nu(C\text{-}H)_{thiazole}$; 1650 (s) ν(C=O); 1630 (m) $\nu(C{=}N)_{imine}$; 1553 (m) $\nu(C{=}N)_{thiazole}$; 1440 (m) $\nu(CH{-}S)_{thiazole}$; 1371 (w), 1326 (m) $\nu(C{=}C)_{thiazole}$; 1200 (m) ν(C–N); 1065 (m) ν(N–O); 975 (w); 915 (w); 871 (m), 793 (m) δ(NH); 404 (m) ν(Cu–N).

2.2.7. Complex [Pd(syn-A)Cl$_2$] (**6**)

$PdCl_2$ (0.0887 g, 0.5 mmol) was dissolved in 6N HCl (3 mL) at 40–50 °C, and ethanol (10 mL) was added. To the resulting transparent light brown solution was added dropwise a hot solution of *syn*-A (0.0936 g, 0.5 mmol), dissolved in 4N HCl (3 mL) and ethanol (7 mL). The reaction mixture was stirred for 45 min under reflux and cooled down to room temperature. The red transparent solution was leaved in the dark place for 70 hours. Brown needle-like single crystals were filtered off, washed with ethanol and diethyl ether and dried in a vacuum desiccator over $CaCl_2$. Yield: 0.101 g (55 %), m.p. ≥ 200 °C (decomp.). Anal. Calc. for $C_5H_5Cl_2N_3O_3PdS$: C, 16.48; H, 1.38; Cl, 19.45; N, 11.53; S, 8.73; Found: C, 16.55; H, 1.45; Cl, 19.15; N, 11.45; S, 8.73 %. ^{1}H NMR, (500 MHz; *d*$_6$-DMSO; δ/ppm): 7.36 (s 1H, $CH_{thiazole}$); 8.64 (br. s 2H, NH_2); 9.28 (br. m 2H, OH, COOH). ^{13}C NMR (125.71 MHz; *d*$_6$-DMSO; δ/ppm): 109.04 C(5); 143.08 C(3); 146.91 C(1); 160.36 C(2); 172.10 C(4). IR data, ν, cm^{-1}: 3620 (br. m) intramolecular hydrogen bond; 3389 (br. m) $\nu(OH)_{COOH}$, 3200 (m) $\nu(NH)_{NH2}$; 3149 (m) $\nu(OH)_{C=N\text{-}OH}$; 2980 (w) $\nu(C\text{-}H)_{thiazole}$; 1667 (m) ν(C=O); 1628 (s) $\nu(C{=}N)_{imine}$; 1540 (m) $\nu(C{=}N)_{thiazole}$; 1435 (m) $\nu(CH{-}S)_{thiazole}$; 1330 (m) $\nu(C{=}C)_{thiazole}$; 1255 (m), 1212 (m) ν(C–N); 1177 (m) δ(NH); 1050 (m) ν(N–O); 946 (w); 845 (m), 807 (m), 747 (m) δ(NH); 395 (m) ν(Pd–N); 318 (m) ν(Pd–Cl).

2.3. Physical measurements

The ^{1}H (^{13}C) NMR spectra were measured on a Varian 300 (300 MHz) and Bruker Avance DRX-500 (500.00 (125.71) MHz) spectrometers in a *d*$_6$-DMSO

solution using TMS as internal standard. The IR spectra were recorded on a Specord M80 in the range 4000–200 cm^{-1} in KBr pellets. UV-vis spectra in DMF solutions of *anti*-A, *syn*-A and its complexes (10^{-3} $mol \cdot L^{-1}$) were recorded on a Specord M40 spectrophotometer in the range 200–900 nm (50000–11000 cm^{-1}) using a 1 mm quartz cell. X-ray photoelectron spectra (XPS) were measured on an ES-2402 device using Mo Kα radiation. Samples were prepared as thin films from an acetone suspension on a 10×10 mm aluminum base plate. Elemental analyses for carbon, hydrogen, nitrogen and sulfur were performed by Carlo Erba Elemental Analyzer Model 1106. The chlorine was measured by Shoniger method.

2.3.1. Single crystal X-ray diffraction

Single crystals of *anti*-A, **1**, **2** and **6** were measured on Bruker SMART APEX2 diffractometer (MoKα radiation, graphite monochromator, λ = 0.71073 Å) at 173 K in the nitrogen stream. Diffraction images were integrated with SAINT program [24]. The obtained intensities were corrected for Lorenz, polarization and absorption using multi-scan technique in SADABS program [25]. All structures were solved by direct methods and refined by full matrix least-square on F^2 using SHELXTL program package [26]. Hydrogen atoms, connected to O and N were located from difference Fourier map and refined without constraints. All other H atoms were put in idealized geometrical positions and refined as a riding model on the host atom. The detailed experimental data is given in Table 1.

Table 1. X-ray crystallographic experimental data for investigated compounds

2.4. Cell culture and growth inhibition (IC_{50})

Mouse aortic cell line (MAEC were used to determine the cytotoxic/cytostatic effects of *anti*-A, *syn*-A and complexes **3**–**6**. Cells were incubated with them for 24 and 48 h under normal conditions in 96 well plates. Initial cell concentration was about 5×10^4 cells/mL in the sample volume of 100 µL. As a culture medium, we used DMEM (Sigma, USA) with 10% FBS (Sigma, USA), 2 mM L-glutamine, and 40 µg/mL gentamicin. Different concentrations (1×10^{-6} – 1.25×10^{-4}) of *anti*-A, *syn*-A, and **3**–**6** were added to cell cultures in 100 µL of media after the period of cell adaptation in normal conditions (5 % CO_2, 100 % humidity, 37 ^oC) during 4 h. In order to evaluate cytotoxic/cytostatic effect of agents MTT-assay was used, that is based on ability dehydrogenases of viable cells to convert yellow water-soluble MTT into blue crystals of formazan that are insoluble. The quantity of formazan (determined by the colorimetric method after

its dissolution in organic solvents) characterizes the intensity of redox processes in cells of culture and is an indirect quantitative characteristic of the active biomass. MTT solution (final concentration is 1 μg/mL) was added to each well before 6 h of ending of incubation period (48 h). After incubation cells were pelleted by centrifugation the plates at 1000 rev / min for 2-3 min, than supernatant was carefully collected and 200 μl of DMSO was added to each well, cells were resuspended and incubated for 10 min at 37°C, whereupon optical density (λ=570 nm) of formazan solution was measured with multiwell spectrophotometer, Synergie Biotec (USA). [28]. Cell counts were performed using a tripan blue dye after 48-hour incubation with agents. The cytotoxic effect was evaluated as percent of live cells relative to control and characterized by IC_{50} index [29], and mitogenic effect was evaluated as percentage increase in the number of cells relative to control.

2.5. Apoptotic level and cell cycle analysis.

Apoptotic level and the distribution of cells in different phases of the cell cycle were assessed by flow cytometry [30]. Cells were plated in 6-well plates at a density of 5×10^4 cells/mL in 5 mL total volume of complete culture medium. Cells were incubated with *anti*-A, *syn*-A, and **3**–**6** in concentration 3.2×10^{-4} M for 48 hours under normal conditions. Cell samples were stained with propidium iodide, which selectively joins with intercalating places in DNA. Staining of cells by flyuorohrom dye PI included the following steps: cells after single rinse in 5 ml of phosphate buffer solution at 1000 rev / min for 10 min, resuspended in 1 ml of hypotonic lysis buffer (0.1% sodium citrate, 0, 1% Triton X-100, 5 mcg / ml PI), ("Sigma Chemical Co", USA). The proportion of cells in different phases of the cell cycle was measured by flow cytometry with argon laser ($\lambda_{excitation}$=488 μm, $\lambda_{emission}$=585/40 μm) (Becton Dickinson, USA) following standard staining. The samples were analyzed with the help of the Mod Fit LT 3.0 (BDIS, USA) software [30]. All measurements were conducted in independent triplicates.

3. Results and discussion

3.1. Syntheses

The presence of several nucleophilic centers in isomeric hydroxyiminoacetic acids *anti*-A and *syn*-A determines their polydenticity and ability for competitive coordination. Therefore, the location of functional groups and synthesis conditions

affect the localization of coordination bonds and the molecular structure of resulted complexes.

The compounds **1–6** were synthesized according to the following scheme:

Scheme for the synthesis of complexes

The interaction of ethanol solutions of metal salts with *anti*-A and *syn*-A in the acidic medium at the component ratios M:L 1:1 and 1:2 leads to the formation of complexes **1–6** with different coordination of ligands. *Anti*-A is coordinated to metal ions in a chelate manner by the nitrogen atoms of the hydroxyimino group and the oxygen atom of the deprotonated carboxyl group. In this case, 2-aminothiazol fragment does not involve in coordination. In the acidic medium, the nitrogen atom of the thiazole ring is protonated with subsequent formation of an H-O-C(O)-C=N-O pseudoheterocycle, based on intramolecular hydrogen bond (NH…O=C), which promotes the stabilization of the molecular structure. In the isomorphous compounds **1** and, **2**, the central metal ion forms an octahedral coordination polyhedron, whose vertices are occupied by the nitrogen and oxygen atoms of ligand, oxygen atoms of three water molecules and sulfate anion Oppositely, in case of complexes **3** and **4,** the metal ion creates a square-planar coordination geometry. Strong acidic synthesis conditions lead to the formation of an extra positive charge on the nitrogen atom of thiazole ring due to its protonation that cause the location of chloride anions in the second coordination sphere (scheme).

Unlike *anti*-A, *sys*-A is coordinated to the metal ion in neutral form by the nitrogen atoms of the hydroxyimino group and thiazole ring. In this case, the central metal ion in the complexes **5** and **6** shows square-planar coordination geometry. Using initial reagent ratio of M:L=1:1, a compound **6** is yielded. The Pd^{2+} ion is surrounded by two nitrogens and two chlorines. It should be noted that irrespective of the reagent ratio, the analogous copper complex can not be obtained, since two *syn*-A molecules completely exchange the chlorine anions in the starting metal salt, forming the compound **5** (scheme).

3.2. Spectroscopy

3.2.1. Infrared spectra

High-frequency region of the IR spectra of *anti*-A and *syn*-A isomers is characterized by absorption bands (ABs), corresponding to the intraligand hydrogen bond at 3620 cm^{-1}, stretching vibrations of ν(NH), ν(OH), ν(C–H) and

$\nu(OH)_{COOH}$ at 3300-3250$_{NH}$, 3150-3180$_{C=N-OH}$, 3025-2935$_{\nu C-H}$, and 2785-2780$_{(OH)COOH}$ cm^{-1} respectively [19, 20, 31–34].

In the frequency range 1700–900 cm^{-1}, a number of characteristic ABs correspond to the vibrations $\nu(C=O)$ (1665/1654), $\nu(C=N)_{imine}$ (1615/1635), $\delta(NH)$ (1575), $\nu(C=N)_{thiaziole}$ (1525/1530), $\nu(CH-S)_{thiazole}$ (1430/1435), $\nu(C=C)$ (1350/1367), $\nu(C-N)$ (1275), $\nu(C-OH)$ (1164/1190), $\nu(N-O)$ (1025/1021). The position shift of these ABs in the spectra of complexes indicate formation of coordination bond. The low-frequency region of the IR spectra of the *anti*-A and *sys*-A compounds (900–200 cm^{-1}) contains the following ABs: $\delta(C-H)$ (888/913), $\nu(C-C)$ (830/823), $\delta(C-H)$ (785/773), $\delta(N-O)$ (688/641), $\delta(C-C)$ (567/556, 477/484, 428/423). However, they are less informative in the sense of bond formation.

The identical IR spectra of the complexes **1** and **2** indicate their isomorphous nature. In the high-frequency region of the spectra, the ABs of the stretching vibrations $\nu(NH)$, $\nu(OH)$, $\nu(C-H)$ of the functional groups NH_2, C=N-OH and C-H at 3200/3312, 3130/3185 and 3005/3000 cm^{-1} respectively, Fig. 1. The new ABs in the spectra at 3420/3400, 2755/2750 and 2617/2650 cm^{-1} are corresponding to the stretching vibrations of coordinated-water O-H bonds, intraligand hydrogen bond and the N-H bond of the protonated nitrogen NH^+ of thiazole ring. The coordination of *anti*-A to the metal ion by oxygen atoms of the carboxyl group and the nitrogen atom of the hydroxyimino group causes a decrease of the frequency of the stretching vibrations $\nu(C=O)$ and $\nu(C=N)_{imine}$ on $\Delta\nu$=14(24) and 25(15) cm^{-1}. The coordination of SO_4^{2-} anions to metal ions confirmed by the presence of ABs at 1085/1100 and 632/618 cm^{-1}, which correspond to $\nu_3(F_2)$ and $\nu_4(F_2)$ of sulfat[35]. In this case, they overlap with vibrations of the N–O bond, which appeared at 1021 cm^{-1} in the spectrum of *anti*-A. In the low-frequency region, the low-intensity ABs at 535/505 and 450/438 cm^{-1} correspond to M–O and M–N bond stretching vibrations [36-38].

Fig. 1. IR spectra of complexes **1–4**

The IR spectra of the complexes **3** and **4** are also identical. The ABs at 3346/3342, 3153/3154, 3020/2994 cm^{-1} are caused by $(NH)_{NH2}$, $(OH)_{C=N-OH}$, $(C-H)_{thiazole}$ bond stretches. The presence of a low-intensity AB of $\nu(NH^+)_{thiazole}$ at 2690/2714 cm^{-1} is common to the spectra of **3** and **4**. N–O bond vibrations in the complexes are shifted by $\Delta\nu$=54/50 cm^{-1} to the high-frequency region in comparison with the spectrum of the ligand. In the low-frequency region ABs of the M–O and M–N stretching vibrations at 515/530, 410/404 cm^{-1} are detected.

Since the OH group of the carboxyl fragment of *syn*-A does not involved in the formation of coordination bond to the metal ion in the complexes **5** and **6**, the position of the AB of the carboxyl group does not change. In this case, the ABs of the thiazole ring are shifted by $\Delta\nu$=50 cm^{-1}, and the (N–O) vibration frequency is higher by $\Delta\nu$=40/25 cm^{-1}. The ABs at 404/395 and 310 cm^{-1} assigned to M–N and M–Cl bond stretches.

3.2.2. UV-vis spectra

The electronic absorption spectrum of the aqueous solution of *anti*-A consists of broad ABs at 45200 cm^{-1} (221 nm), 39700 cm^{-1} (251 nm) and 34700 cm^{-1} (288 nm). The decomposition of the spectrum into Gaussians gave four peaks at 45200, 39700, 34700 and 31800 cm^{-1}, which assigned to the intraligand $\pi\rightarrow\pi^*$ (C=N) electron transitions of thiazole ring, $\pi\rightarrow\pi^*$ (C=N) of hydroxyiminogroup and $\pi\rightarrow\pi^*/n\rightarrow\pi^*$ (C=O) of carboxyl group [19, 20, 31, 34, 38, 39] (Fig. 2*a*).

The UV-vis spectrum of the aqueous solution of *syn*-A contains of two broad ABs at 44250 cm^{-1} (226 nm) and 38300 cm^{-1} (261 nm). The decomposition of the spectrum into Gaussians revealed four peaks at 44250, 38300, 35000 and 32200 cm^{-1} (Fig. 2*b*), which correspond to the intraligand electron transitions $\pi\rightarrow\pi^*$ (C=N) of thiazol ring, $\pi\rightarrow\pi^*$ (C=N) of hydroxyiminogroup and $\pi\rightarrow\pi^*/n\rightarrow\pi^*$ (C=O) of carboxyl group [19, 20, 31, 34, 38, 39].

Fig 2. UV-vis spectra of aqueous solutions of *anti*-A (*a*) and *syn*-A (*b*) with decomposition into Gaussian components

The spectra of the *anti*-A and *syn*-A isomers differ in the position of the ABs of intraligand electron transitions, which are explained by different orientation of chromophore groups relative to hydroxyiminogroup (C=N-OH). The frequency of the electron transitions $\pi\rightarrow\pi^*$ of thiazole ring and (C=N) hydroxyiminigroup of *anti*-A is shifted by $\Delta\nu$=+950, +1400 cm^{-1} to the high-frequency region in comparison with *syn*-A. Oppositely, the position of the Gaussians corresponding to the electron transitions $\pi\rightarrow\pi^*/n\rightarrow\pi^*$ (C=O) of *anti*-A is shifted by $\Delta\nu$=-300, -400 cm^{-1} to the low-frequency region.

The UV-vis spectra of aqueous solutions of the complexes **1** and **2** are similar. They differ only in the position of the ABs, which correspond to ligand-to-metal charge transfer transitions (LMCTT), at 28100 cm^{-1} (complex **1**) and 28300 cm^{-1} (complex **2**). In the range of 45000–38000 cm^{-1}, the ABs of the $\pi\rightarrow\pi^*$ (C=C, C=N) electron transitions of thiazole ring and $(C=N)_{imine}$ at 44580, 42970, 39400 cm^{-1} are detected. In this case, the bathochromic shift by $\Delta\nu$=-(620-300) cm^{-1} of these bands

relative to pristine *anti*-A is observed. It could be explained by protonation of the nitrogen atom of the thiazole rings and coordination of the hydroxyiminogroup to the metal ion. The ABs that assigned to the π→π* transitions of C=O are also shifted by Δν=+70 cm^{-1} and -250 cm^{-1}, which is probably caused by the formation of a metallocycle. The ABs of d-d transitions appears at 19500, 15100 cm^{-1} in **1** and 21800, 15000 cm^{-1} in **2**.

The spectra of the aqueous solutions of the complexes **3** and **4** are also similar, which indicates the same coordination mode of the ligand to the central metal ion (Table 2). The LMCTTs of these complexes appears at 28900 cm^{-1} (for **3**) and 28720 cm^{-1} (for **4**) and d-d transitions at 16750 cm^{-1} and 24700 $см^{-1}$ respectively.

Table 2. UV-Vis spectra of synthesized compounds (ν, cm^{-1})

The UV-vis spectra of the aqueous solutions of the complexes **5** and **6** are similar. The ABs of electron transitions π→π* of thiazole ring and $(C=N)_{imine}$ are at 44720, 43150 and 36160 cm^{-1} in the complex **5** and at 44700, 43000, 36160 cm^{-1} in the complex **6**. They undergo a hypsochromic shift by Δν=+470/450 and 1160 cm^{-1} relative to the ABs of starting *syn*-A, which indicates their coordination to the central metal ion. Besides, in the spectra of the complexes there are LMCTTs at 29100 and 28800 cm^{-1}. The position of the d-d transitions at 16700 cm^{-1} in **5** and 24400 cm^{-1} in **6** is typical of the square-planar shape of the coordination unit.

3.3.3. ^{1}H (^{13}C) NMR and X-ray photoelectron spectra

The ^{1}H NMR spectra of the compounds *anti*-A and *syn*-A contain a broadened singlet of amine group at 7.30 ppm, and the oxime and carboxyl groups appear as one broadened signal in a range of 12.40-13.0 ppm due to protons exchange. It should be noted that the positions of the singlets of the 5-H protons of the thiazole ring in the spectra of *anti*-A and *syn*-A differ noticeably (*anti*-A, 7.56 ppm; *syn*-A, 6.84 ppm), Fig. 3 *a*, *b*. An analogous dependence was noted for the corresponding ethyl ethers of *anti*-A and *syn*-A [40]. The ^{13}C NMR spectra of the *anti*-A and *syn*-A contains five carbon signals, the position of which differ from each other by (δ = 8.45 (C5), 3.85 (C3), 3.57 (C1), 0.13 (C2), 1.79 (C4) ppm.

Fig. 3. ^{1}H NMR spectra of *anti*-A (*a*) and *syn*-A (*b*)

In the ^{1}H NMR spectrum of the complex **6**, the signals from the 5-H protons of the thiazole ring and amine group undergo a shift of Δδ=+0.52 and +1.34 ppm,

respectively, to the downfield in comparison with starting *syn*-A, which is due to the coordination of the thiazole ring to the metal ion. In this case, the broadened singlet of oxime and carboxyl group protons shifts by Δδ=-3.15 ppm to the upfield, which is associated with the formation of intraligand hydrogen bonds and coordination of the oxime nitrogen atom to the palladium ion.

In contrast to the compound **6**, the signals from the 5-H proton of the thiazole ring and amine group in the ^{1}H NMR spectrum of the complex **4** shift slightly by Δδ=+0.01 and +0.23 ppm to the downfield, indicating a lack of coordination of the thiazole ring to the palladium ion. Besides, in the spectrum of the complex there is a broadened singlet at 8.17 ppm, which corresponds to the proton NH^{+} at the nitrogen atom of the thiazole ring, Fig 4. The protonation of the thiazole ring is also confirmed by the IR spectra of this complex and by the X-ray analysis of the complexes **1** and **2**, in which coordination of *anti*-A is carried in a similar manner.

Fig. 4. ^{1}H NMR spectrum of compound **4**

Carbon signals of C(1), C(2) in the ^{13}C NMR spectra of complexes **4**, **6** are shifted upfield by (δ = -1.6/-0.67 and -4.68/-4.36 ppm, whereas carbon signals of C(3), C(4), C(5) are shifted downfield relative to the starting isomers by (δ = 2.28/1.19, 5.8/3.94, 1.57/3.01 ppm, due to their coordination to the central metal ion, Fig. 5.

Fig. 5. ^{13}C NMR spectra of *anti*-A, *syn*-A and compounds **4**, **6**

It is known that coordination of the ligand to the central metal ion can be determined by X-ray photoelectron spectra. Therefore, we used XPS spectroscopy for studying the coordination mode of *anti*-A and *syn*-A to palladium (complexes **4**, **6**) and copper (complexes **3**, **5**) ions.

Analysis of the spectra showed that the N1s line of *anti*-A and *syn*-A consists of three components with E_{bond} = 400.10/399.71, 400.95/400.70, 401.71/401.50 eV, which correspond to the three non-equivalent nitrogen atoms NH_2, $C=N_{thiazole}$ and $C=N_{imine}$, Fig. 6. In the spectra of complexes **4**, **6** E_{bond} of these groups increased by 0.02/0.06 (NH_2), 0.19/0.37 ($C=N_{thiazole}$) and 0.81/0.91 ($C=N_{imine}$) eV. Their values are 400.12/399.77, 401.14/401.07, 402.52/402.41 eV. Based on this it is evident that E_{bond} of ($C=N_{thiazole}$) and ($C=N_{imine}$) are greatest in complex **6**, while in complex **4** only most increased the value of E_{bond} ($C=N_{imine}$). This indicates to polytypic coordination of *anti*-A and *syn*-A to the metal ions according to the proposed synthesis scheme.

Fig. 6. N1s lines of anti-A, syn-A and complexes 4, 6 in X-ray photoelectron spectra

In the XPS spectra of complexes **3**, **5**, the values of component N1s are 400.15/399.81, 401.32/400.93, 402.59/402.38 eV. Similar to palladium complexes, in compounds 3, 5 the values of N1s increased by 0.05/0.10 (NH_2), 0.37/0.23 ($C=N_{thiazole}$) and 0.88/0.88 ($C=N_{imine}$) eV, indicating the similar coordination of *anti*-A and *syn*-A to copper ions.

The value E_{bond} $Pd3d_{5/2}$ and $Pd3d_{3/2}$ in the complexes **4**, **6** are 340.11/345.35 and 339.70/344.87 eV, while the E_{bond} Cu $2p_{3/2}$ are 932.70 and 933,10 eV in copper complexes **3**, **5**, indicating the divalent state of metal ions, Fig.7.

Fig. 7. $Pd3d_{5/2}$, $Pd3d_{3/2}$ and $Cu2p_{3/2}$ lines in XPS

3.3. X-ray diffraction study

3.3.1. anti-A

A sulfate salt of the *anti*-A was crystallized from the 0.4M solution of H_2SO_4. The compound crystallized in a monoclinic crystal system (space group $P2_1/n$) with two organic cations, sulfate anion and lattice water molecule in the asymmetric unit (Fig. 8). Thiazole rings in both molecules are planar. The mean deviation from least square plane amount to 0.003 and 0.008 Å for C1/N1/C2/C3/S2 and C6/N4/C7/C8/S3 correspondingly. 2-Hydroxyiminoacetate groups are found in *anti*-conformation in both molecules that confirms by torsion angles C5-C4-N2-O5 = -176.72 ° and C10-C9-N5-O8 = -174.82°. The carboxylate groups in both molecules are protonated showing values of C-O bond lengths characteristic for the presence of pronounced single and double bonds (See Table S1, ESI). The whole molecules have a non planar structure with most significant deviation from between thiazole and 2-hydroxyiminoacetate groups. The dihedral angles between C1/N1C2/C3/S2 and C4/C5/O7/O6/N2/O5 planes amount to 15.74°. The second molecule has a twice higher divergence of 31.95° between C6/N4/C7/C8/S3 and C9/C10/O9/O10/N5/O8 planes. In both molecules, the hydrogen atoms were found on thiazole nitrogens from difference Fourier map, confirming the cationic nature of species. Mentioned hydrogen atoms involved in intramolecular H-bonds (Table SX, ESI) with carboxylate C=O groups, forming pseudoheterocycles N1/C2/C4/C5/O7/H1 and N4/C7/C9/C10/O9/H4. In the crystal structure all structural units are connected in a complicated 3D Framework of intermolecular H-bons (See Table S2, ESI).

Fig. 8. Molecular structure of sulfate salt of the *anti*-A. Dashed lines indicate hydrogen bonds

3.3.2. [Co(anti-A)(H$_2$O)$_3$SO$_4$] (**1**) and *[Ni(anti-A)(H$_2$O)$_3$SO$_4$]* (**2**)

Compounds **1** and **2** crystallized in the same space group *P2$_1$/n*. Similar unit cell parameters and composition revealed the isostructural nature of the compounds. The crystallographic independent part contains one molecule of complex (Fig. 9). The metal atoms have a nearly regular MNO_5 (M – Ni, Co) octahedral coordination geometry with typical M—O and M—N bond lengths (Table S3, S5, ESI).

Fig. 9. Molecular structure of complexes **1** and **2** with labeling scheme. Dashed lines indicate hydrogen bonds

The coordination environment of the central atom consists of O5 and N1 from the ligand molecule, coordinated in the bidentate chelate manner. Additional four oxygen atoms originate from coordinated sulfate anion and three water molecules. Analyzing the torsion angles C1-C2-O1-O7 (-177.43° for 1 and -176.76° for 2) one can conclude about the anti-conformation of the 2-hydroxyiminoacetate group in both cases. The metallarings M1-N1-C2-C1-O5 are planar with deviation from least square plane of 0.0212 Å for **1** and 0.0247 Å for **2**. Remarkably that chelatation to the metal center also influenced the geometry of the ligand molecule. Thus, decreasing of dihedral angle between thiazole and 2-hydroxyiminoacetate groups to 6.39(14)° for **1** and 6.55(14)° for **2** is pointed on planar configuration of the coordinated ligand molecule. Intramolecular hydrogen bonds N2—H2N…O6, O7—H7O…O2 and O8—H82O…O3 are additionally stabilizing the molecule of complex. As in the case of anti-A, the complex 3D Framework of hydrogen bonds is found in the crystal structure (Table S4 and S6, ESI).

3.3.3. [Pd(syn-A)Cl$_2$] (**6**)

Using $PdCl_2$ in the synthesis leads to formation of complex **6** that crystallized in orthorhombic symmetry (space group *Pna2$_1$*). The asymmetric unit contains one molecule of complex and lattice water molecule (Fig. 10). The central Pd atom revealed slightly distorted square-planar $PdCl_2N_2$ coordination geometry (Table S7, ESI) with mean deviation from least-square plane of 0.0104 Å. In contrast to Co(II) and Ni(II) complexes, a five membered planar metallaring Pd1/N1/C1/C3/N2 is formed due to the strong affinity of Pd(II) to nitrogen. This forces the switch of ligand conformation from *anti-* to *syn-*. This evidenced by C2/C1/N1/O1 torsion angle of 0.49°. The molecule of complex is not planar

because of dihedral angle between O2—C2—O3 carboxylate and remaining moiety of 34.9(1)°. Besides, the compound is additionally stabilized by intramolecular H-bonds O1—H1O—Cl2 and N3—H32N—Cl1 (Table S8, ESI). In the crystal structure, the 3D framework of H-bonds is found.

Fig. 10. Molecular structure of **6** with labeling scheme. Dashed lines indicate hydrogen bonds

3.4. Cell culture tests

Our study showed that *anti*-A and *syn*-A demonstrated multidirectional effects on endothelial cells. *Syn*-A showed mitogenic effect by stimulating dose-dependently proliferation of cells in the concentration range $8x10^{-6}$–$1.25x10^{-4}$ M (average effect was 23.7%±7.2% *vs.* control). At the same concentration range, *anti*-A slightly inhibited proliferation of endothelial cells (Fig. 11 *a*, *b*), but had opposite effect in concentration $3.20x10^{-4}$ M.

Cytofluorometric analysis revealed that *syn*-A increased 1.8-fold ($p<0.05$) cells population of the proliferative pool (G_2/M+S) *vs.* control and *anti*-A effects (Table 3). This effect was associated with increase number of cells both in G_2/M ($p<0.05$) and S ($p<0.001$) phases of cell cycle and no change in G_0/G_1 cell population. *Anti*-A increased number of cells in S phase ($p<0.01$), decreased - in G_2/M ($p<0.05$), but didn't affect number of cells in the proliferative pool (G_2/M+S) as well as in G_0/G_1 phases of cell cycle.

In spite of multidirectional effect of tested compounds on cells proliferative activity, both *anti*-A and *syn*-A ($3.20x10^{-4}$ M) induced anti-apoptotic effect *vs.* control. *Anti*-A and *syn*-A have reduced the percentage of apoptotic cells in 3- and 2.6-fold ($p<0.01$), respectively (Fig. 12).

Fig. 11. The influence of *anti*-A with compounds 3, 4 (a) and *syn*-A with complexes 5, 6 (b) on the endothelial cells proliferative activity. MTT–test

Fig. 12. The influence of *anti*-A, *syn*-A and complexes **3**-**6** on the level of endothelial cells apoptotic index: ^ *$p<0.05$ – vs. control, * $p<0.01$ – vs. control*

Table 3. Cells distribution in phases of cell cycle under the influence of tested *anti*-A, *syn*-A and complexes **3-6**

The complexation of *anti*-A and *syn*-A with transition metals changed their effectiveness. Complex **3** and **4** had more profound anti-proliferative effect *vs.* *anti*-A. However, complex **4** was more effective in comparison with complex **3**

(fig. 11 *a*). Complex **3** slightly increased number of cells in the proliferative pool (G_2/M+S) (1.1-fold, $p<0.05$), which was associated with increase - in S phase ($p<0.05$) and no change in G_2/M *vs.* control. The number of cells in G_0/G_1 phase was decreased by complex **3** *vs.* control, *anti*-A and complex **4** effects. Influence of complex **4** on cell cycle phase was similar to effect of *anti*-A (Table 3). Redistribution of cells in cell cycle phases described for *anti*-A, complexes **3** and **4**, may result in cells entrance in postsynthetic checkpoint and autophagic death [41].

The incubation of endothelial cells with complex **3** led to reduced apoptotic cells percent. Complex **4** didn't affect apoptotic level of cells *vs.* control, but increased apoptotic cells percent *vs. anti*-A (Fig. 12).

We could not detect cytotoxic effect for a*nty*-A, while both complexes (**3** and **4**) had cytotoxic effect ($IC_{50}= 1.33x10^{-4}$ M for **3** and $IC_{50}=2.5x10^{-5}$ M for **4**).

Complexes of metal with syn-A (**5** and **6**) induced opposite effect in comparison to *syn*-A: compound **6** did not affect cells percent in G_0/G_1 phase *vs.* control, but increase *vs*. syn-A effect. Redistribution in G_2/M and S was the most pronounced relatively to control and compound *syn*-A. The population of cells in S phase exceeded control and syn-A effects, in 10- and 1.2-fold, respectively (Table 3). It was associated with 3.2- and 10-fold ($p<0.01$) increase number or apoptotic cells *vs*. control and *syn*-A effects, respectively (Fig. 8). The similar effects were described for compounds that modify activity of p53 and can lead to checkpoint of cells conversion in G_2 and initiation of apoptosis [42]. Complex **5** had slight cytostatic effect (1.1-fold) *vs*. control and complex 6, and more profound (1.8-fold, $p<0.01$) *vs*. *syn*-A.

4. Conclusions

We showed that *anti*-A and *syn*-A coordinate bidentately to Co^{2+}, Ni^{2+}, Cu^{2+} and Pd^{2+} ions yielding chelate-type complexes. *Anti*-A coordinates to the central metal ion by the oxygen atom of the deprotonated carboxyl group and the nitrogen atom of the oxime group. Oppositely, *syn*-A coordinates to the central metal ions by two nitrogen atoms of the oxim group and thiazole ring. The molecular structures of synthesized complexes were stabilized by intramolecular hydrogen bonds, forming so-called pseudoheterocycles. All complex compounds form stable solutions in neutral medium, which makes it possible to use them as potential biologically active substances.

When studying the biological effect of the compounds *anti*-A and *syn*-A on the main cell target (endotheliocytes), it has been found that *syn*-A exhibits

mitogenic and antiapoptotic effect, whereas *anti*-A causes inhibition of proliferation almost in all tested diapason.

Under the influence of complex compounds on endothelial cells, an increase in the antiproliferative activity of the complexes **3–6** in comparison with starting complexing agents is observed. Thus the activity of the *syn*-A-based complexes is higher than that of the analogous complexes with *anti*-A. The complex compounds **3** and **4** show pronounced cytotoxic action, and **6** has cytotoxic and proapoptotic properties. For the complex **5**, cytostatic effect has been established. The "arrest" of conversion from S to G_2 was detected for all tested compounds that can be evidence of malfunction in DNA replication or deregulation in endogenic signals of cell cycle in endotheliocytes associated with hypoxia and further HIF-1 activation. Profile of tested compounds influence on endothelial cells denotes its potential utilization as pharmacological angiogenesis directed drug.

Acknowledgements

Prof. Ludmila Garmanchuk is thankful to the Dr I. Goot, University of London for the kindly providing of Mouse aortic cell line.

Appendix A. Supplementary data

The crystal structures of compounds *anti*-A and 1, 2 and 6 have been submitted to the CCDC and have been allocated the deposition numbers CCDC 987450-987453 for compounds *anti*-A, **1**, **2** and **6**, respectively. These data can be obtained free of charge via www.ccdc.cam.ac.uk/conts/retrieving.html (or from the Cambridge Crystallographic Data Centre, 12 Union Road, Cambridge CB21EZ, UK; fax: (+44) 1223-336-033). Supplementary data associated with this article can be found, in the online version, at doi:

References

[1] S.R. Pattan, S.B. Pawar, S. B., S.S. Vetal, U.D. Gharate, S.B. Bhawar, Indian Drugs 49 (2012) 5–12.
[2] E. Meggers, Curr. Opin. Chem. Biol. 11 (2007) 287–292.
[3] M. Navarro, C. Gabbiani, L. Messori, D. Gambino, Drug Discov. Today 15 (2010) 1070–1078.
[4] S. Rafique, M. Idrees, A. Nasim, H. Akbar, A. Athar, Biotechnol. Mol. Biol. Rev. 5 (2010) 38–45.
[5] S. Annadurai, R. Martinez, D.J. Canneya, T. Eidem, P.M. Dunman, M. Abou-Gharbia, Bioorg. Med. Chem. Lett. 22 (2012) 7719–7725.

[6] N. Singh, U.S. Sharma, N. Sutar, S. Kumar, U.K. Sharma, J. Chem. Pharm. Res. 2 (2010) 691–698.
[7] X. Zhang, H.O. Yang, Y. Ding, Adv. Materials Res. 396–398 (2012) 2489–2493.
[8] A. Gallardo-Godoy, J. Gever, K.L. Fife, B.M. Silber, S.B. Prusiner, A.R. Renslo, J. Med. Chem. 54 (2011) 1010–1021.
[9] J. Das, J.A. Furch, C. Liu, R.V. Moquin, J. Lin, S.H. Spergel, K.W. McIntyre, D.J. Shuster, K.D. O'Day, B. Penhallow, C.-Y. Hung, A.M. Doweyko, A. Kamath, H. Zhang, P. Marathe, S.B. Kanner, T.-A. Lin, J.H. Dodd, J.C. Barrish, J. Wityak, Bioorg. Med. Chem. Lett. 16 (2006) 3706–3712.
[10] P. Carmeliet, R.K. Jain, Nat Rev Drug Discov. 10(6) (2011) 417-427
[11] T.N. Crawford, D.V. Alfaro III, J.B. Kerrison, E.P. Jablon, Curr. Diabetes Rev. 5 (2009) 8–13.
[12] J. Folkman, Semin. Oncol. 28 (2001) 536–542.
[13] M. Rajappa, P. Saxena, J. Kaur, Adv. Clin. Chem. 50 (2010) 103–121.
[14] I.E. Koutroubakis , G. Tsiolakidou, K. Karmiris, E.A. Kouroumalis, Inflamm. Bowel Dis. 12 (2006) 515–523.
[15] A. Messmer-Blust, X. An, J. Li, Trends Cardiovasc. Med. 19 (2009) 252–256.
[16] S. Szabo, X. Deng, G. Tolstanova G, T. Khomenko, B. Paunovic, L. Chen, M. Jadus, Z. Sandor, Curr. Pharm. Des. 17 (2011) 1633–1642.
[17] A.L. Harris, Nat. Rev. Cancer 2 (2002) 38–47.
[18] X. Lin, C.A. David, J.B. Donnelly, M. Michaelides, N.S. Chandel, X. Huang, U. Warrior, F. Weinberg, K.V. Tormos, S.W. Fesik, Y. Shen, Proc. Natl. Acad. Sci. U.S.A. 105 (2008) 174–179.
[19] I. Georgieva, N. Trendafilova, G. Bauer, Spectrochim. Acta A 63 (2006) 403–415.
[20] C.O. Onindo, T.Y. Sliva, T. Kowalik-Jankowska, I.O. Fritsky, P. Buglyo, L.D. Pettit, H. Kozlowski, T. Kiss, J. Chem. Soc. Dalton Trans. (1995) 3911–3915.
[21] C.B. Botta, W. Cabri, E. Cini, L. De Cesare, C. Fattorusso, G. Giannini, M. Persico, A. Petrella, F. Rondinelli, M. Rodriquez, A. Russo, M. Taddei, J. Med. Chem. 54 (2011) 2165–2182.
[22] K.D. Hardy, F.P. Harrington, A.V. Stachulski, J. Chem. Soc. Perkin Trans. 1. 6 (1984) 1227–1235.
[23] M.O. Suita, A.M. Ikeda, Y.M. Nishinomiya, US Pat (1985) 4503234 A.
[24] Bruker, SAINT, Bruker AXS Inc., Madison, Wisconsin, USA, 2002.
[25] G.M. Sheldrick, SADABS, University of Gottingen, Germany, 2003.
[26] Bruker. SHELXTL, Bruker AXS Inc., Madison, Wisconsin, USA, 2001.

[27] A.L. Spek, PLATON, University of Utrecht, The Netherlands, 2002.
[28] T. Mosmann, J. Immunol. Methods 65 (1983) 55–63.
[29] M.C. Alley, D.A. Scudiero, A. Monks, M.L. Hursey, M.J. Czerwinski, D.L. Fine, B.J. Abbott, J.G. Mayo, R.H. Shoemaker, M.R. Boyd, Cancer Res. 48 (1988) 589–601.
[30] I. Nicoletti, G. Migliorati, M.C. Pagliacci1, F. Grignani1, C. Riccardi, J. Immunol. Methods 139 (1991) 271–279.
[31] A.A. Mokhir, E. Gumienna-Kontecka, J. Świątek-Kozlowska, E.G. Petkova, I.O. Fritsky, L. Jerzykiewicz, A.A. Kapshuk, T.Yu. Sliva, Inorg. Chim. Acta 329 (2002) 113–121
[32] M. Kandaz, S.Z. Çoruhlu, Transition Met. Chem. 27 (2002) 877–883.
[33] D. Jayaraju, A.K. Kondapi, Current Science 81 (2001) 787–792.
[34] B.K. Singh, U.K. Jetley, R.K. Sharma, B.S. Garg, Spectrochim. Acta A 68 (2007) 63–73.
[35] C.G. Efthymiou, V. Nastopoulos, C. Raptopoulou, A. Tasiopoulos, Bioinorg. Chem. Appl. 2010 (2010) doi: 10.1155/2010/960571.
[36] M.S.S. Babu, P.G. Krishna, K.H. Reddy, G.H. Philip, J. Chil. Chem. Soc. 54 (2009) 339–344.
[37] M.S.S. Babu, P.G. Krishna, K.H. Reddy, G.H. Philip, Indian J. Chem. 47A (2008) 1661–1665.
[38] W.-K. Dong, Sh.-Sh. Gong, Y.-X. Sun, J.-F. Tong, J. Yao, J. Structural Chem. 52 (2011) 1018–1024.
[39] E. Canpolat, M. Kaya, Polish J. Chem. 77 (2003) 961–967.
[40] M.O. Suita, A.M. Ikeda, Y.M. Nishinomiya, US Pat (1987) 4680390.
[41] W. Bursch, Cell Death Differentiation 8 (2001) 569–581.
[42] R.D. Dinnen, L. Drew, D.P. Petrylak, Y. Mao, N. Cassai, J. Szmulewicz, P. Brandt-Rauf, R.L. Fine, J. Biol. Chem. 282 (2007) 26675–26686.

Table 1

X-ray crystallographic experimental data for investigated compounds

Compound	***anti*-A**	**1**	**2**	**6**
Брутто-формула	$C_{10}H_{14}N_6O_{11}S_3$	$C_5H_{11}CoN_3O_{10}S_2$	$C_5H_{11}N_3NiO_{10}S_2$	$C_5H_7Cl_2N_3O_4PdS$
Молекулярна маса	490.45	396.21	396.00	382.50
Crystal system, space group	*Monoclinic, $P2_1/n$*	*Monoclinic, $P2_1/n$*	*Monoclinic, $P2_1/n$*	*Orthorhombic, $Pna2_1$*
Unit cell dimensions (Å)	a = 7.0929(13) b = 21.166(4) c = 12.230(3) β = 104.906(10)	a = 6.8185(3) b = 13.6661(8) c = 13.8939(9) β = 102.961(4)	a = 6.7770(2) b = 13.6007(4) c = 13.8496(4) β = 102.798(2)	a = 7.2574(14) b = 12.233(2) c = 12.487(3)
Volume (Å^3)	1774.3(6)	1261.68(12)	1244.83(6)	1108.6(4)
Z, Calculated density (g/cm^3)	4, 1.836	4, 2.086	4, 2.113	4, 2.292
μ, mm^{-1}	0.495	1.751	1.954	2.345
F(000)	1008	804	808	744
θ range for data collection (º)	1.92 to 26.38	2.12 to 26.43	2.13 to 26.53	2.33 to 26.42
Limiting indices	$-8 \le h \le 8$ $-21 \le k \le 26$ $-15 \le l \le 9$	$-8 \le h \le 8$ $0 \le k \le 17$ $0 \le l \le 17$	$-8 \le h \le 8$ $-17 \le k \le 14$ $-17 \le l \le 17$	$-8 \le h \le 9$ $-15 \le k \le 15$ $-13 \le l \le 15$
Reflections collected/unique	8866/3595 [*R(int)*=0.0282]	2704	9883/2580 [*R(int)* =0.0341]	7900/1912 [*R(int)* = 0.0651]
Data/parameters ($I > 4\sigma(I)$)	3595/307	2704/231	2580/220	1912/163
Goodness-of-fit on F^2	1.082	1.087	1.038	1.091
R [$I > 4\sigma(I)$], *Rw (all data)*	0.0340, 0.1050	0.0340, 0.0933	0.0336, 0.0865	0.0365, 0.0830
Largest diff. peak and hole (eÅ^{-3})	*0.308 and -0.407*	0.318 and -0.511	0.391 and -0.483	0.875 and -0.649

Table 2. UV-Vis spectra of synthesized compounds (ν, cm^{-1})

compounds	π→π* thiazole ring	π→π* $(C=N)_{thiazole}$	π→π* $(C=N)_{imine}$	π→π*/n→π* (C=O)	LMCTT	d-d
anti-A	45200	39700	34700	31800	–	–
syn-A	44250	38300	35000	32200	–	–
1	sh 44580, 42970	39400	34770	31400	28100	19500, 15100
2	sh 44580, 42970	39400	34450	31225	28300	21800, 15000
3	47900, 42000	39500	35200	33500	28900	16750
4	sh 44500, 42800	37400	35250	33000	28720	24700
5	sh 44720, 43150	39500	36160	32100	30800	16700
6	44700, 43000	39300	36160	32500	28800	24400

Sh, shoulder absorption band; LMCTT, Ligand-to-Metal Charge Transfer Transition

Table 3.

Cells distribution in phases of cell cycle under the influence of tested *anti*-A, *syn*-A and complexes **3-6**

compounds	G_0/G_1	G_2/M	S	G_2/M+S
Control	67.39±1.2	29.07±2.16	3.54±0.01	32.61±2.17
anti-A	67.05±2.06	19.24±1.02[a]	13.71±1.04[b]	32.95±2.06
syn-A	41.64±1.02[b],[c]	36.29±2.09[a]	22.07±0.74[b]	58.36±2.83[b]
3	62.40±1.06[a],[c]	21.12±1.16	16.49±1.34[b]	37.61±2.52[a],[c]
4	68.66±1.32	14.08±0.80[b]	17.26±1.65[b]	31.34±2.45
5	72.07±0.34[a],[d]	18.64±1.00[a],[d]	9.29±0.33[a],[d]	27.93±1.33[a],[d]
6	65.09±0.22[d]	6.36±0.07[b],[d]	28.25±2.18[b],[d]	34.61±0.95[d]

[a] $p<0.05$; [b] $p<0.01$ – vs. control; [c] $p<0.05$ vs. a*nti*-A; [d] $p<0.05$ – vs. *syn* A

Figures

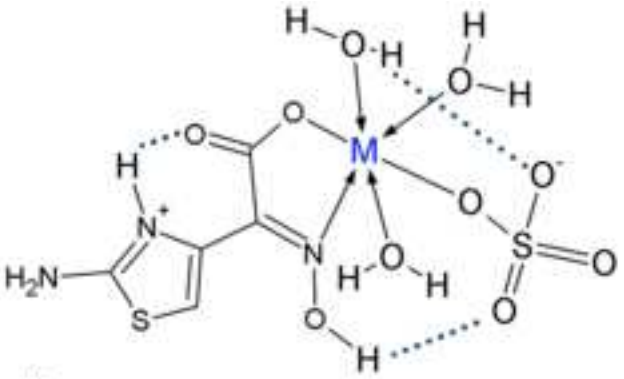

M = Co^{2+} (1)

M = Ni^{2+} (2)

$[MH_2L(H_2O)_3SO_4]$

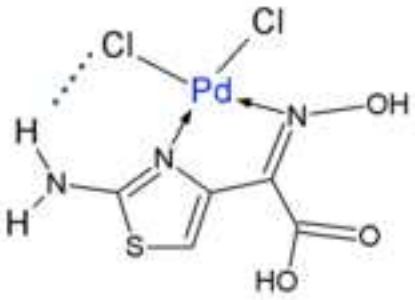

$[Pd(H_2L)Cl_2]$ (6)

M:L 1:1

+ $M(NO_3)_2 \times 6H_2O$

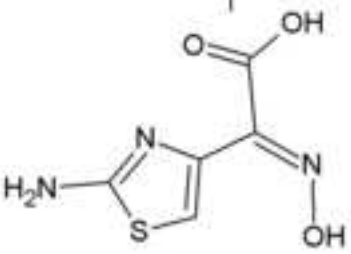

Anti-A

M:L 1:1

+ $PdCl_2$

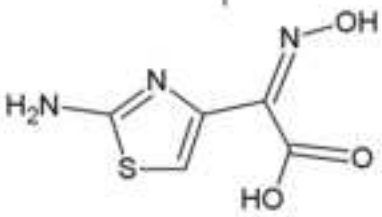

Syn-A

+ MCl_2

M:L 1:2

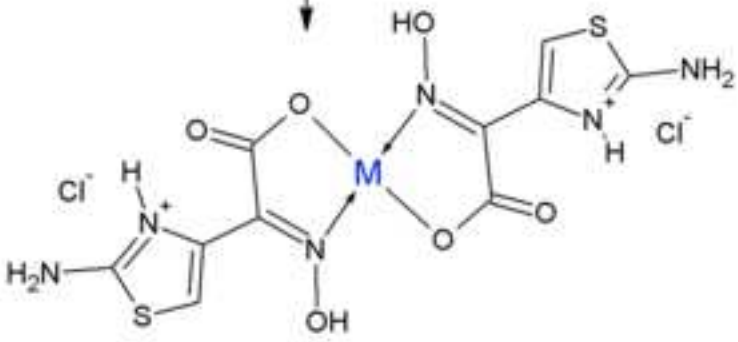

M = Cu^{2+} (3)

M = Pd^{2+} (4)

$[M(H_2L)_2]Cl_2$

+ $CuCl_2 \times 2H_2O$

M:L 1:2

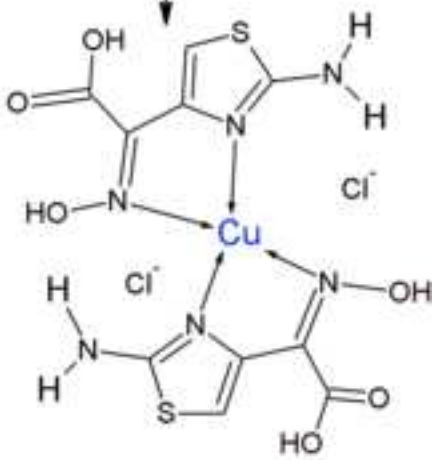

$[Cu(H_2L)_2]Cl_2$ (5)

Figures

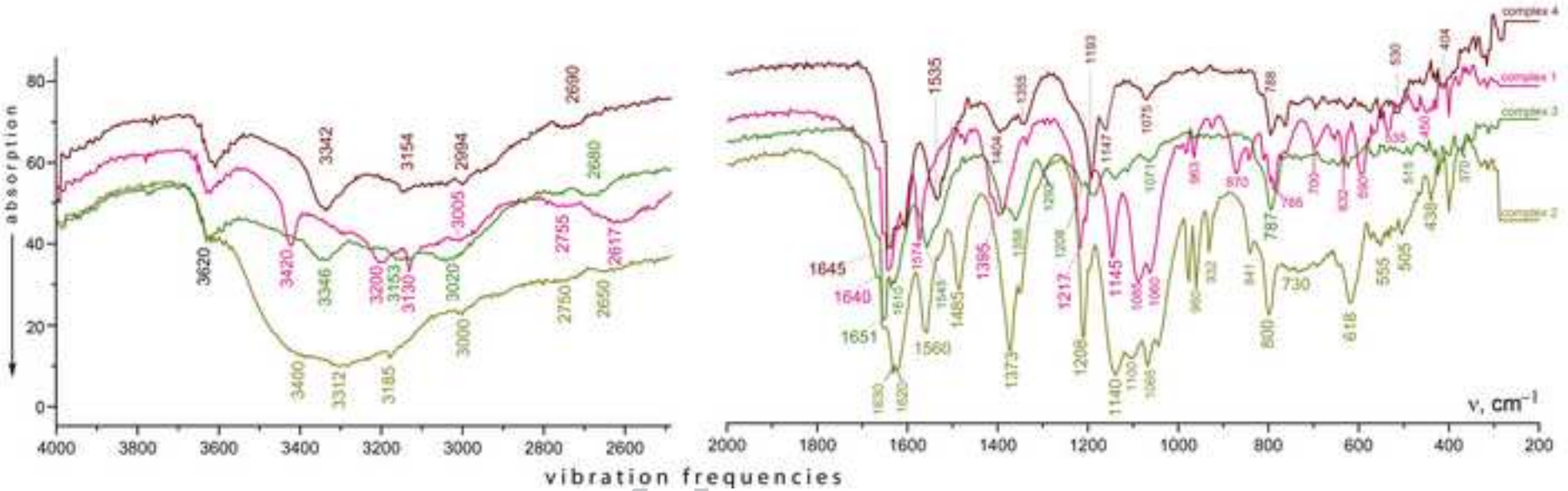

Figures

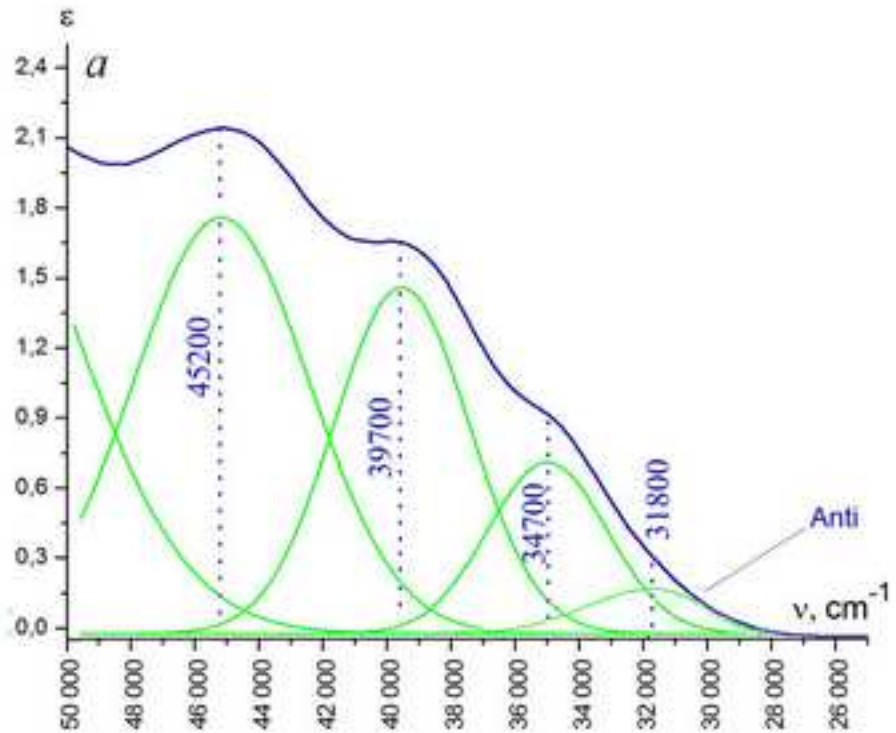

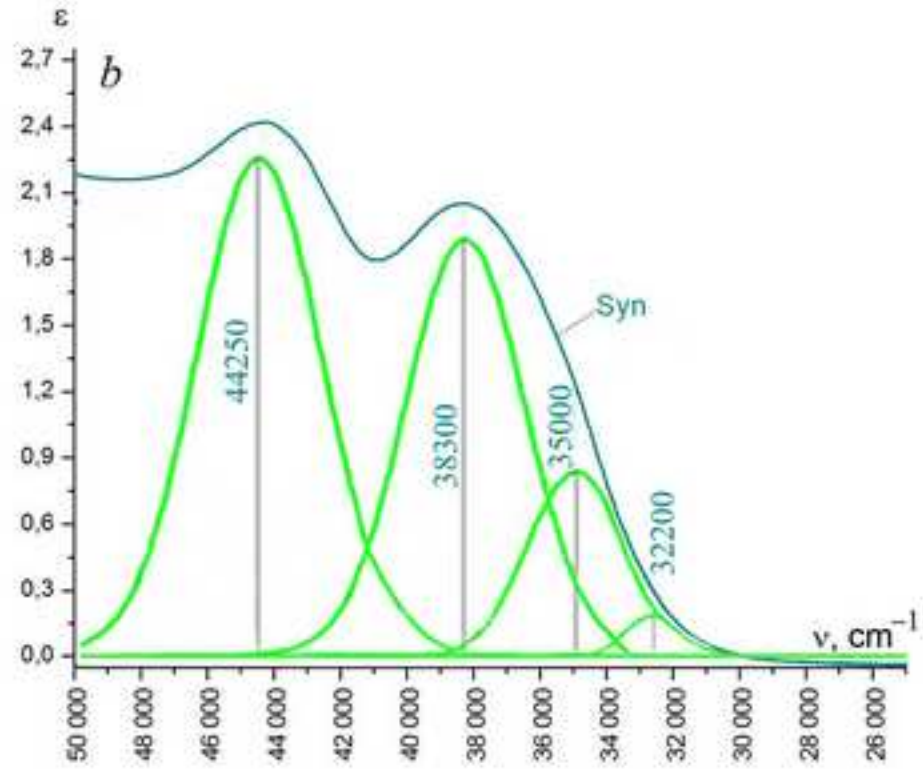

Figures

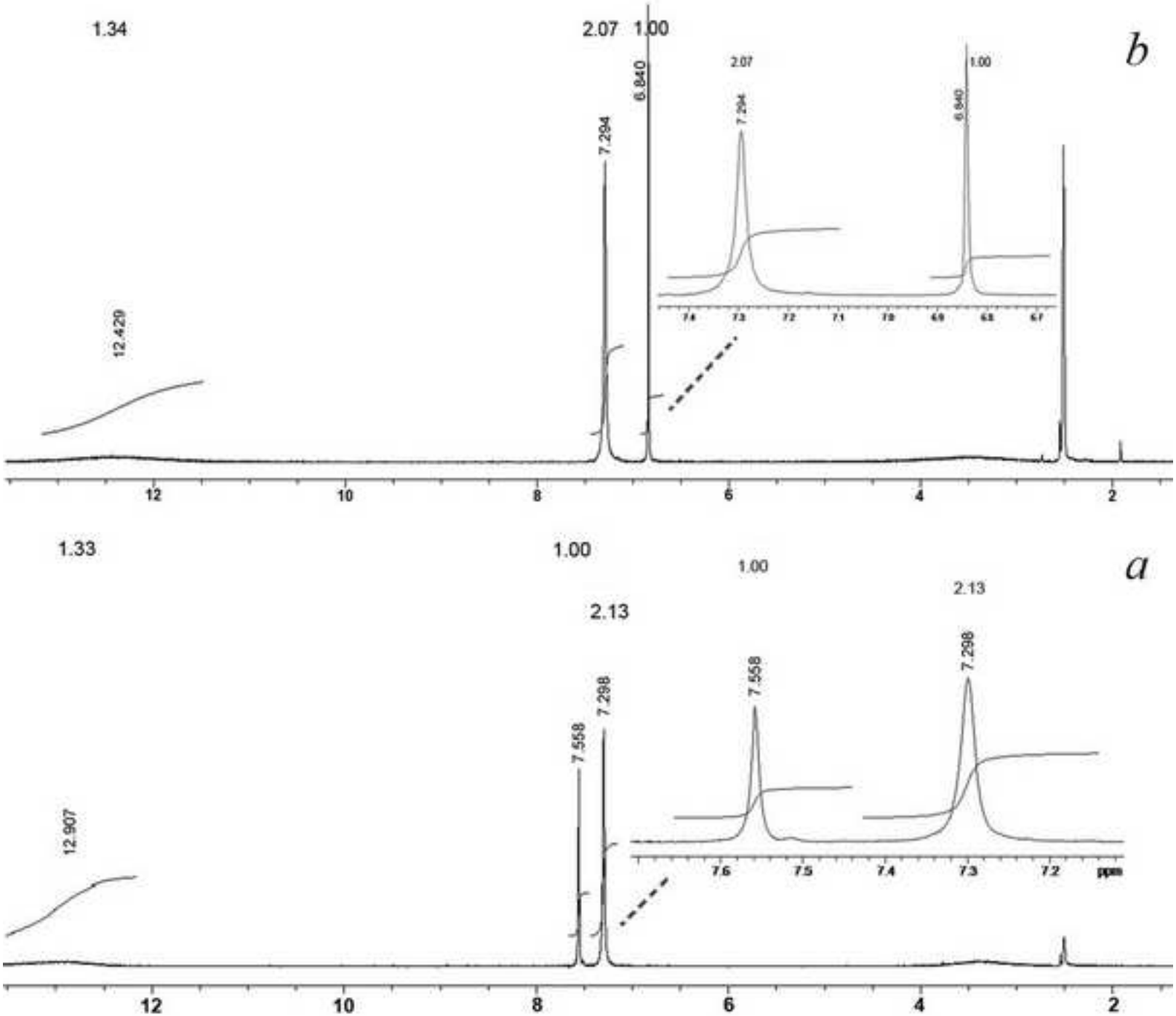

Figures

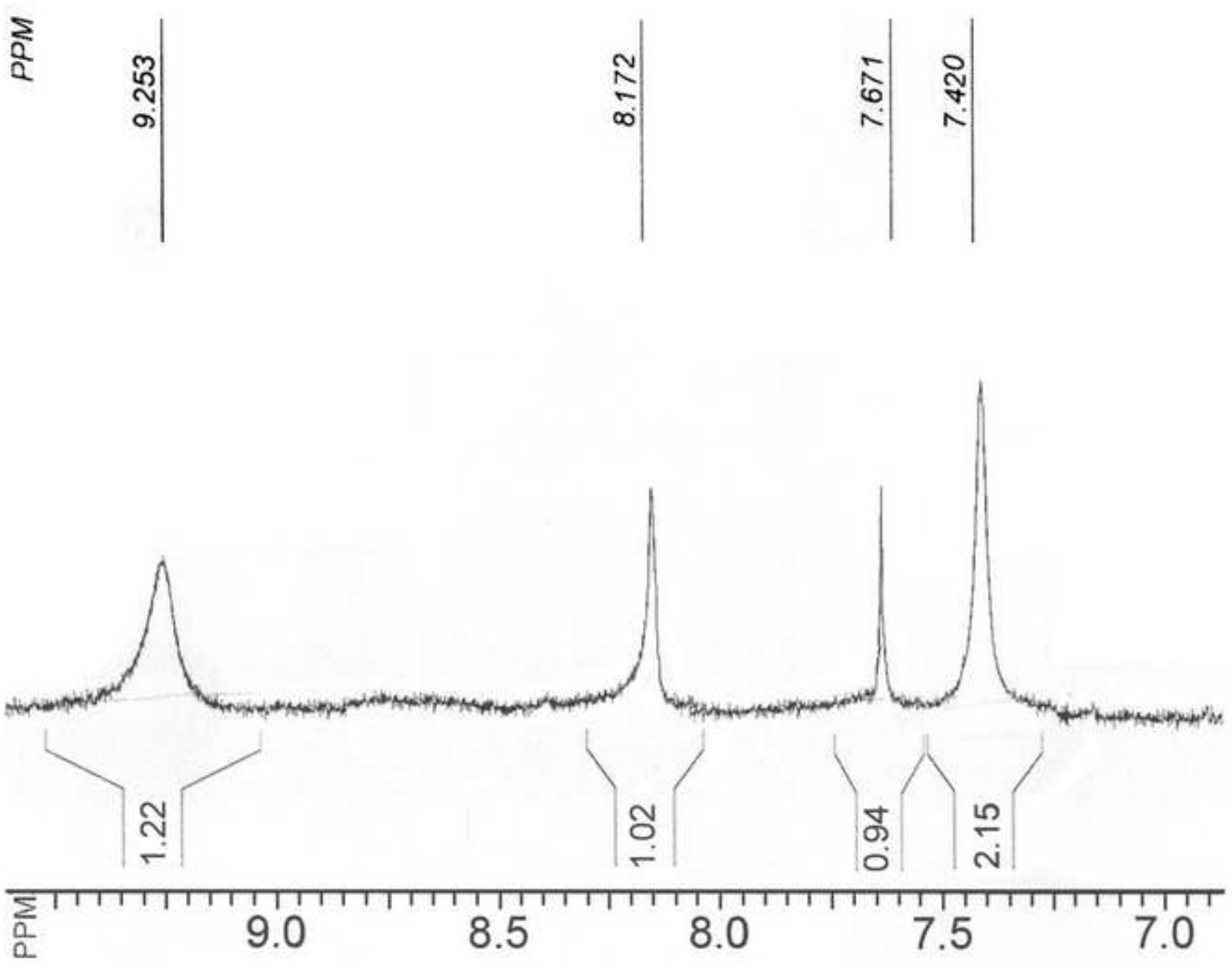

Figures

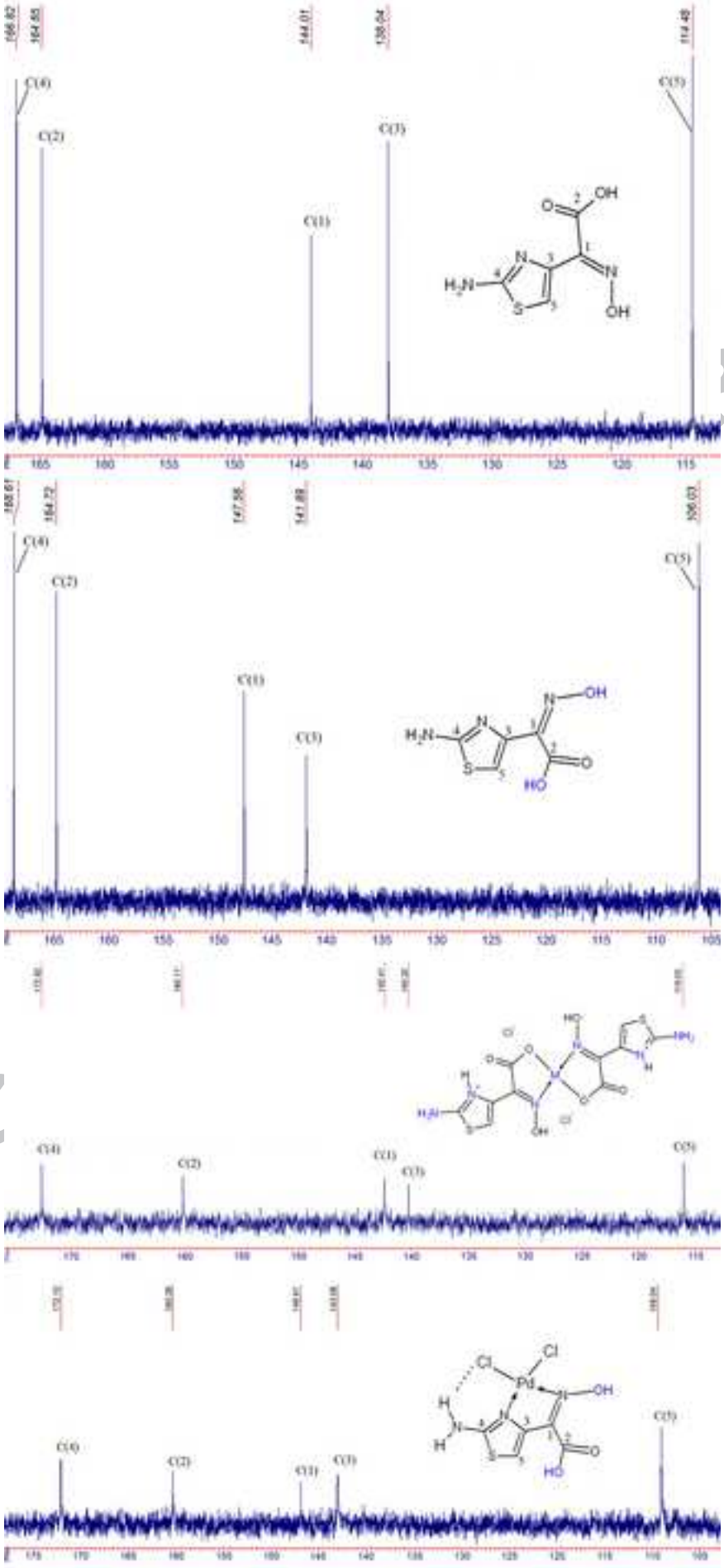

Figures